DEVELOPMENT OF ICE ACCRETION AND ANTI-ICING SYSTEM SIMULATION CODE

Seiji Nishio* and Sumio Kato*
***Kawasaki Heavy Industries, LTD**

Keywords: *ice accretion, anti-icing, simulation code*

Abstract

Ice accretion on surfaces of aircraft components in icing condition can affect aerodynamic performance and stability of the aircraft, and jeopardize flight safety. Therefore, some types of ice protection system have been developed in order to counteract ice accumulation. Numerical simulation for the prediction of ice accretion and performance of ice protection system is helpful to design the system and reduce the total cost and the development period. In order to design the anti-icing system of an aircraft, the ice accretion and anti-icing system simulation code (KHI code) has been developed. This simulation code calculates flow field, collection efficiency, surface temperature, water mass flow rate, and ice shapes of a two dimensional airfoil, based on a flight condition and meteorological condition. In this paper, the overview and validation results of this code are presented.

Nomenclature

A_c = cross surface area of the skin, m^2
$alfa$ = angle of attach, deg
c = chord length, m
C_p = specific heat, J/(kg K)
Cp = pressure coefficient
d_{ice} = ice thickness, m
f_{frz} = freezing fraction
f_{wet} = wetness factor
h = heat transfer coefficient, $W/(m^2 K)$
h_{in} = internal heat transfer coefficient, $W/(m^2 K)$
k = thermal conductivity of skin, W/(m K)
L_f = latent heat of fusion, J/kg
L_v = latent heat of evaporation, J/kg
LWC = liquid water content, kg/m^3
M = molecular mass, kg/kmol
m = Mach number
$\dot{m}$ = mass flux, $kg/(m^2 s)$
MVD = medium volumetric diameter, μ m
P = pressure, Pa
P_v = partial vapor pressure of water, Pa
Pr = Prandtl number
Q = heat flux, W/m^2
Q_{anti} = heat flux from anti-icing system, W/m^2
Q_{conv} = heat loss by external convection, W/m^2
Q_{htr} = power density of heater, W/m^2
Q_{sens} = sensible heat required to warm runback water, W/m^2
Q_{wall} = heat flux coming out of skin, W/m^2
s = surface distance, m
Sc = Schmidt number
T = temperature, K
T_{ref} = reference temperature, K
t = time, sec
U = velocity, m/s
x, y = spatial coordinate, m
β = local collection efficiency
Δs = surface distance between impact points, m
Δy = distance at start between two trajectories, m

η = recovery factor
ρ = density, kg/m^3

Subscripts

e = evaluated at edge of boundary layer
evap = evaporation from surface
ice = ice
imp = impingement on surface
bair = bleed air
rin = runback water entering an element
rout = runback water leaving an element
s = skin
w = water
∞ = freestream condition

1 Introduction

Supercooled liquid water droplets may exist in atmospheric cloud where the ambient temperature is below freezing. When an aircraft flies through such a cloud, the water impinging on surfaces of the aircraft components may freeze, resulting in subsequent buildup of ice. Ice growth on the surface of an aircraft can lead to degradation of the aerodynamic performance and stability, and jeopardize the flight safety. Because of its importance, various ice protection systems have been developed. These systems can be classified in two categories: de-icing system and anti-icing system. Anti-icing system works continuously during a flight in the icing condition and prevents a protected surface from ice build up, either by evaporating the impinging water or by allowing it to runback and freeze on non-critical surface. De-icing system works periodically and sheds the small ice buildups, either by mechanical or thermal means.

Numerical simulation codes can reduce costs and a period to design these ice protection systems and simulate the entire icing envelope, which it is difficult for ground and/or flight icing test to accomplish. Many icing simulation code, such as LEWICE, ANTICE, CANICE, and FENSAP-ICE have been developed and utilized for design and certification of ice protection system of an aircraft [1].

These simulation codes can predict ice shapes and performance of ice protection system in icing conditions and be utilized to design of ice protection system and to decide whether ice protection system is needed, or not on each component. The ice accretion and anti-icing system simulation code (KHI code) has been developed in order to design a thermal anti-icing system of an aircraft.

In this paper, the function and mathematical model of this code are presented. Numerical results of KHI code are compared with experimental data and other numerical results.

2 Ice Accretion and Anti-icing Model

The KHI code consists of 4 regions: (1) flow field calculation, (2) droplet trajectory and impingement calculation, (3) heat and mass balance calculation, and (4) Ice shape calculation. Two-dimensional model is used for each calculation. Figure 1 shows the general outline of this simulation code.

(1) Flow Field Calculation

The first calculation of this simulation code is that of flow field around an arbitrary two-dimensional body. The potential flow solution around an airfoil is calculated by the panel method. This airflow is inviscid and incompressible. The Panel method is practical in the point of time-consuming, compared with a Navier-Stokes solver.

This flow solution is used to determine the external convective heat transfer coefficient. The external convective heat transfer coefficients on the airfoil surface are calculated by the integral boundary layer method, same as that of LEWICE [3] and CANICE [2]. The heat transfer coefficients on the ice accretion area are calculated by the similar method to LEWICE [3] using an equivalent sand grain factor.

(2) Droplet Trajectory and Impingement Calculation

Each droplet trajectory, starting at unperturbed upstream of the airfoil, is calculated by the Lagrangian Method, based on the flow

solution. The local collection efficiency β is found from the ratio of the distance at the start point of trajectory calculation to the surface distance between impact points, which is shown in Equation (1).

$$\beta = \frac{\Delta y}{\Delta s} \tag{1}$$

A single droplet particle or arbitrary droplets distribution can be selected as input in this code.

(3) Heat and Mass Balance Calculation

The calculation of heat and mass balance starts at the stagnation point. Any water that doesn't freeze in an each node is assumed to flow downstream to a next node. In this calculation, water droplet kinetic energy, external heat convection, latent heat (evaporation and fusion) and sensible heat of water, and anti-icing heating are included. Energy balance equations are shown in Equation (2) to (8). It is assumed that the temperature of the skin is the same as the runback water temperature.

$$Q_{imp} - Q_{evap} - Q_{conv} - Q_{ice} + Q_{sens} + Q_{wall} = 0 \tag{2}$$

$$Q_{imp} = \dot{m}_{imp}\left\{C_{p,w}\left(T_{\infty} - T_{ref}\right) + \frac{U_{\infty}^{\,2}}{2}\right\} \tag{3}$$

$$Q_{evap} = \dot{m}_{evap}\left\{C_{p,w}\left(T_s - T_{ref}\right) + L_v\right\} \tag{4}$$

$$Q_{conv} = h_e\left(T_s - T_e - \frac{\eta U_e^{\,2}}{2C_{p,e}}\right) \tag{5}$$

$$Q_{ice} = \dot{m}_{ice}\left\{C_{p,ice}\left(T_s - T_{ref}\right) + L_f\right\} \tag{6}$$

$$Q_{sens} = \dot{m}_{rin}C_{p,w}\left(T_{s,rin} - T_{ref}\right) - \dot{m}_{rout}C_{p,w}\left(T_s - T_{ref}\right) \tag{7}$$

$$Q_{wall} = Q_{anti} + A_c k\frac{dT_s}{dx^2} \tag{8}$$

This simulation code can calculate the runback ice, which is generated when water is not completely evaporated by the anti-icing system and freeze on the unprotected surface.

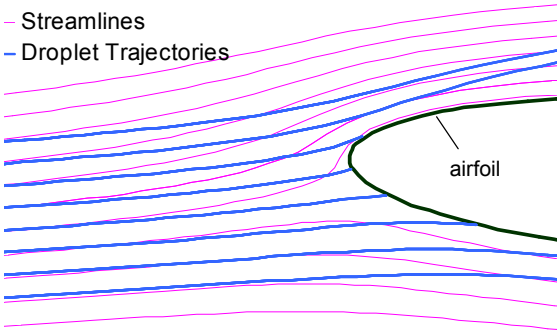

(a) Airflow and Water Droplets Trajectory

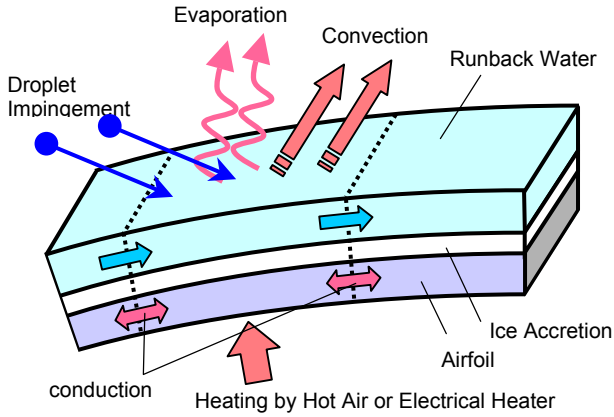

(b) Heat and Mass Balance on a Airfoil

Figure 1 Model of Ice Accretion and Anti-icing System

Anti-icing heating is based on hot air system or electro-thermal heater. In the case of electro-thermal heater, anti-icing heat flux is power density of heater, as shown in Equation (9).

$$Q_{anti} = Q_{htr} \tag{9}$$

In the case of hot air anti-icing system, internal heat transfer coefficient is calculated based on the internal configuration and hot air condition. Staged arrays of piccolo holes are regarded as arrays of nozzles and the average heat transfer coefficient is calculated in the region of jet impingements [4]. The anti-icing heat flux is given by

$$Q_{anti} = h_{in}\left(T_{bair} - T_s\right) \tag{10}$$

Mass balance equation includes impingement, evaporation, runback, and solidification of the water. Impingement rate of water is obtained by

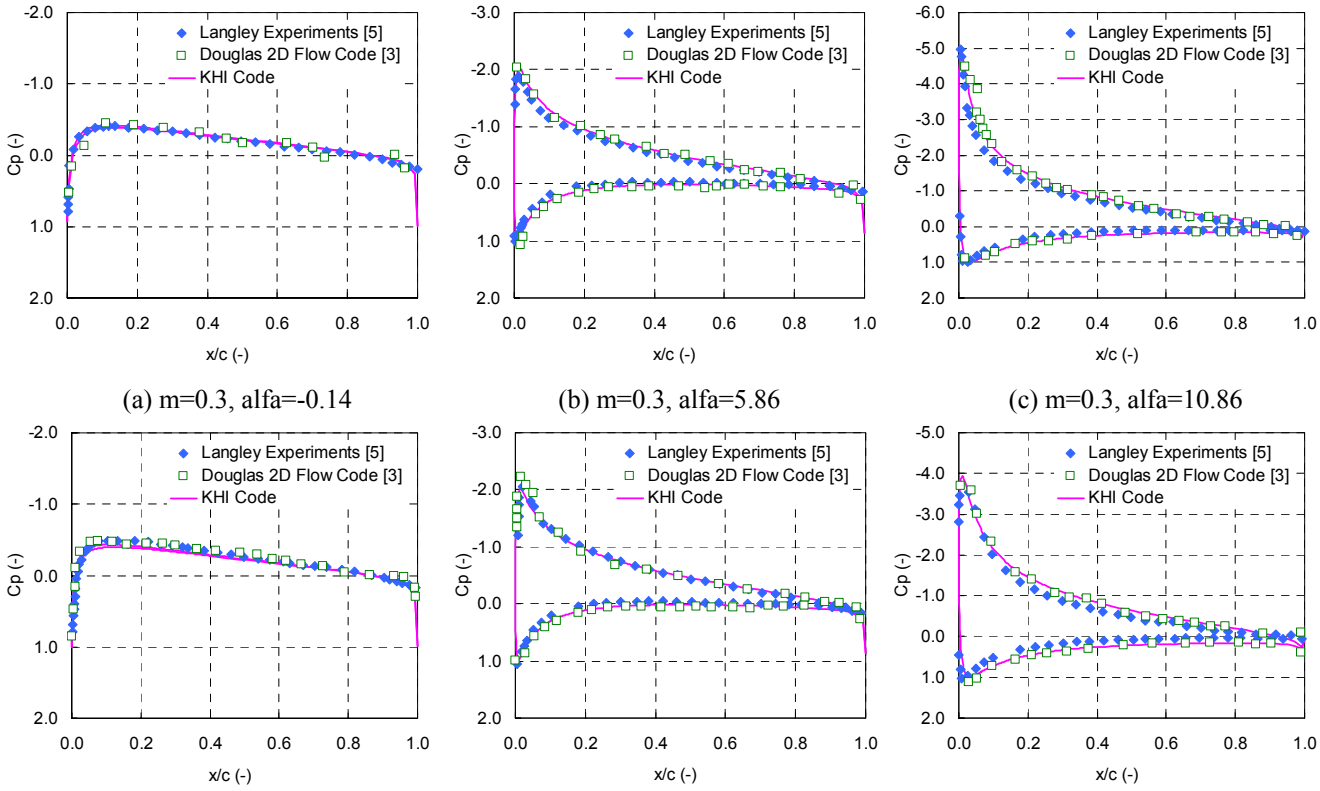

(a) m=0.3, alfa=-0.14 (b) m=0.3, alfa=5.86 (c) m=0.3, alfa=10.86

(d) m=0.5, alfa=-0.14 (e) m=0.5, alfa=5.86 (f) m=0.5, alfa=10.86

Figure 2 Comparison of the pressure coefficient around the NACA0012 airfoil

$$\dot{m}_{imp} = LWC \cdot \beta \cdot U_{\infty} \tag{11}$$

$$\dot{m}_{rout} = \left(1 - f_{frz}\right)\left(\dot{m}_{imp} - \dot{m}_{evap} + \dot{m}_{rin}\right) \tag{14}$$

Evaporation rate of water is obtained from the heat transfer coefficient and the ratio of Prandtle number and Schmidt number [10], which is shown in Equation (12). A wetness factor f_{wet} is defined as the fraction of the skin surface that is wetted by the runback water (rivulet). $P_{v,w}$ is the saturated vapor pressure on the water surface and $P_{v,e}$ is the local vapor pressure at the edge of the boundary layer.

$$\dot{m}_{evap} = f_{wet} \frac{h_e}{Cp_e}\left(\frac{Pr}{Sc}\right)^{2/3} \frac{M_w}{M_{air}}\left(\frac{P_{v,w} - P_{v,e}}{P_e - P_{v,w}}\right) \tag{12}$$

The mass flux of runback water and the ice growth rate are obtained from the following Equations (13) and (14) [10]. The term f_{frz} is the freezing fraction, which is defined as the ratio of liquid water that freezes in an element and ranges from 0 (no ice) to 1 (no runback water).

$$\dot{m}_{ice} = f_{frz}\left(\dot{m}_{imp} - \dot{m}_{evap} + \dot{m}_{rin}\right) \tag{13}$$

(4) Ice Accretion Shape Calculation

Ice thickness during a specific time interval is calculated based on the ice growth rate given from the heat and mass balance calculation. Ice is assumed to grow normal to the clean airfoil or the ice surface covering the airfoil. The thickness of the ice layer, which grows on each time interval, is given by

$$d_{ice} = \frac{\dot{m}_{ice}\Delta t}{\rho_{ice}} \tag{15}$$

This ice thickness is added to the geometry of the clean airfoil to form the iced airfoil geometry. The KHI code has multi-time step calculation capability. In this calculation, airflow, droplet trajectories, heat and mass balance, and increasing ice thickness are re-calculated on the iced airfoil at each time interval and ice thickness are added to the previous iced airfoil geometry.

3 Results and Discussion

3.1 Validation of the Flow Field Calculation

In Figure 2, pressure coefficients on the NACA0012 airfoil (c=0.625m), which were calculated by the KHI code, are compared with wind tunnel test data and the Douglas 2D Flow Code calculation results [3, 5]. The Douglas 2D Code was employed as the program for the flow field calculation of the LEWICE and calculated the two-dimensional potential flow [5].

The pressure coefficients are well predicted by the KHI code for angle of attack up to 11 degrees and Mach numbers up to 0.5 and calculation results with the KHI code agree well with the experimental data and another calculation results.

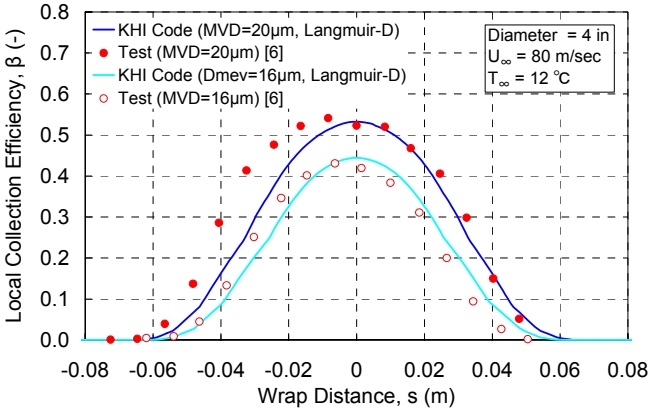

Figure 3 Comparison of the local collection efficiency test results and calculations on the 4in cylinder

Table 1 Ambient condition for the calculation of the local collection efficiency on the NACA0012 airfoil

Angle of Attach	Static Temperature	Free-stream Velocity	Medium Volume Diameter	Liquid Water Content
alfa	T_∞	U_∞	MVD	LWC
deg	℃	m/sec	μm	kg/m^3
0.0	-6.67	44.7	20	0.00078
0.0	-6.67	89.4	20	0.00039
2.0	-6.67	89.4	20	0.00039
4.0	-6.67	89.4	20	0.00039

3.2 Validation of the Droplet Impingement Characteristics Calculation

Calculation results of local collection efficiency on a cylinder and the NACA0012 airfoil are compared with test results and

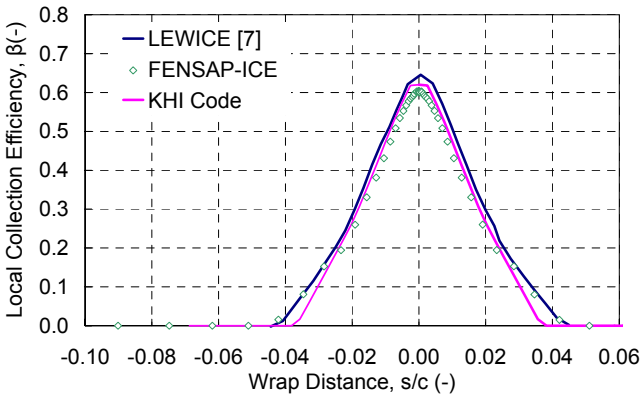

(a) alfa=0deg, U_∞=89.4m/s

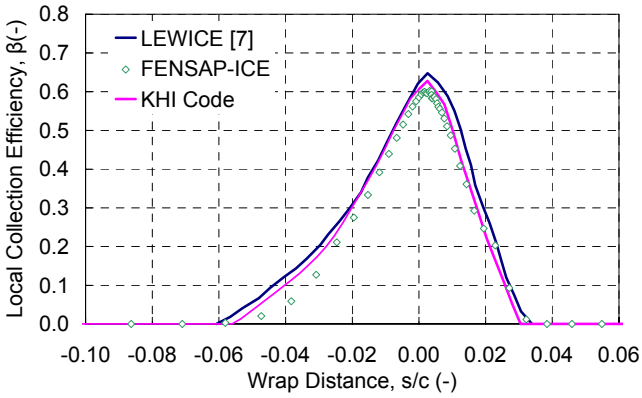

(b) alfa=2deg, U_∞=89.4m/s

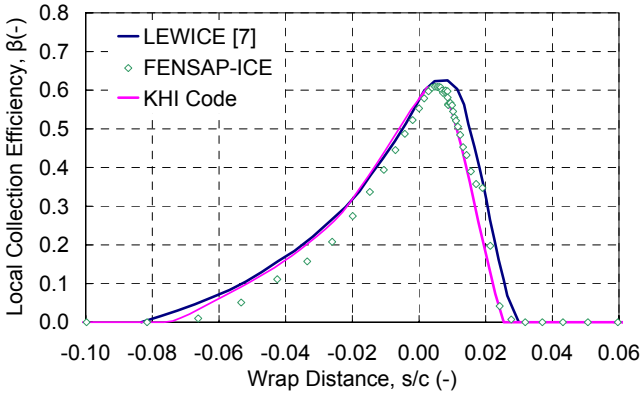

(c) alfa=4deg, U_∞=89.4m/s

Figure 4 Comparison of the local collection efficiency on the NACA0012 airfoil surface with MVD solution

calculation results with other simulation codes.

Figure 3 shows the comparison of the local collection efficiencies of the cylinder with 4in diameter, between the test results conducted in the NASA Lewis Icing Research Tunnel [6] and KHI code numerical results, which considered Langmuir-D distribution of the droplets. The local collection efficiencies calculated by KHI code agree well with test results.

Numerical results of the local collection efficiency on the NACA0012 airfoil by the KHI code were compared with numerical results by LEWICE [7], ANTICE [8], and FENSAP-ICE. The Local collection efficiencies of FENSAP-ICE were calculated by KHI side. Numerical

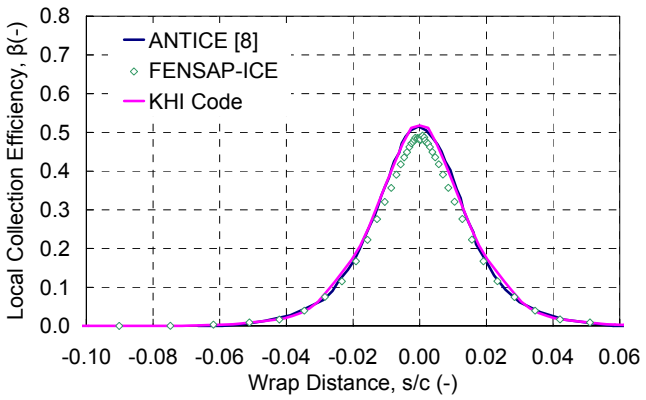

(a) alfa=0deg, U_∞=44.7m/sec

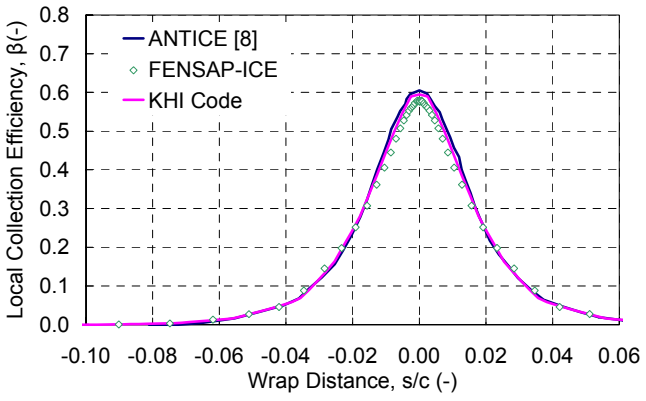

(b) alfa=0deg, U_∞=89.4m/sec

Figure 5 Comparison of the local collection efficiency on the NACA0012 airfoil surface with Langmuir-D distribution

Table 2 Icing condition for the calculation of the surface temperature and water mass flow rate on the NACA0012 airfoil

Icing Condition	Static Temperature	Free-stream Velocity	Medium Volume Diameter	Liquid Water Content	Angle of Attach
	T_∞	U_∞	MVD	LWC	alfa
	°C	m/sec	μ m	kg/m^3	deg
22A, 22B	-7.6	44.7	20	0.00078	0.0
35A	-18.8	44.7	20	0.00078	0.0
67A, 67B	-21.76	89.4	20	0.00055	0.0

Table 3 Wrap position and power densities of the heaters

Heater	wrap position (cm)		power densities (W/m^2)				
	start	end	22A	22B	35A	67A	67B
H1	-9.360	-5.550	9920	2635	12090	20150	8370
H2	-5.550	-3.010	10230	2945	11780	21700	11935
H3	-3.010	-0.470	32550	4030	34100	32550	10850
H4	-0.470	1.435	46500	4805	46500	43400	15190
H5	1.435	3.975	18600	2945	23250	26350	9920
H6	3.975	6.515	6980	3410	6665	18600	12865
H7	6.515	10.325	10230	2325	12710	18600	8680

conditions are listed in Table 1. Figure 4 shows the comparison on a single particle size based on the medium volumetric diameter (*MVD*) and Figure 5 shows the comparison on the Langmuir-D distribution of droplets. There are small variances among the local collection efficiencies calculated by each solver. The numerical results by the KHI code are mean values among these results.

3.3 Validation of the Thermodynamic Characteristics Calculation

For validation of the heat and mass balance calculation, the numerical results are compared with the experimental data and numerical results by ANTICE and CANICE [2,8]. The experimental data were obtained with the NACA0012 airfoil, 6-ft span and 36 in chord, equipped with an electro-thermal ice protection system at the leading edge. Table 2 lists the test

conditions and Table 3 lists wrap coordinates and power densities of each of heaters.

The electro-thermal ice protection system has six layers of different thermal conductivity and thickness. Because the model of the KHI code assume that temperature across skin thickness is constant, an equivalent thermal conductivity (0.9182 W/m/K) and an equivalent skin

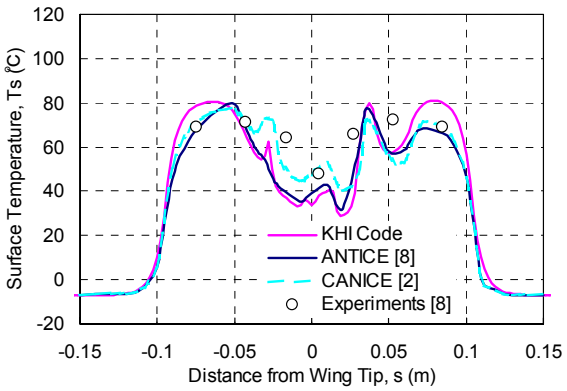

(a) Surface temperature

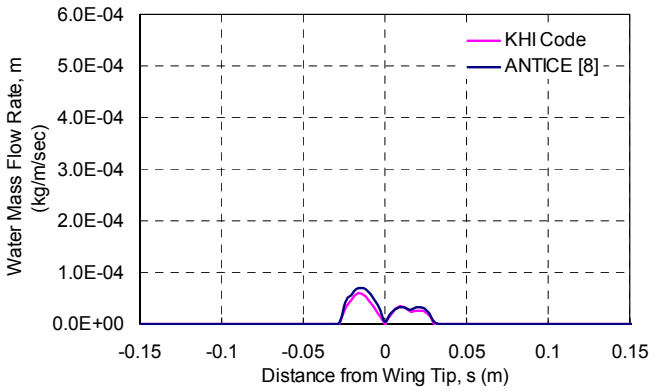

(b) Water mass flow rate

Figure 6 Comparison of experiments and predictions for Case#22A

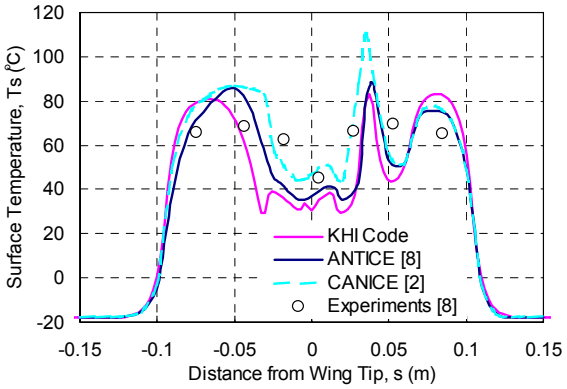

(a) Surface temperature

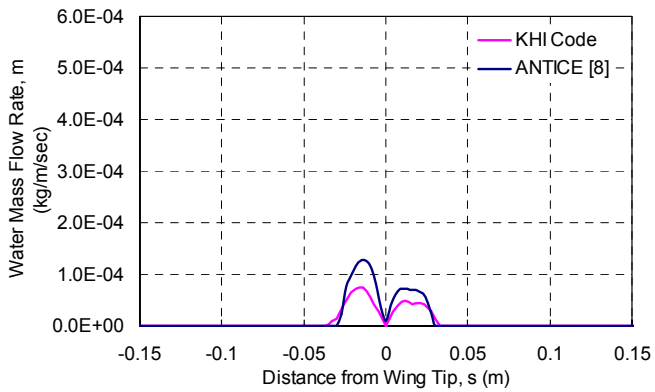

(b) Water mass flow rate

Figure 7 Comparison of experiments and predictions for Case#35A

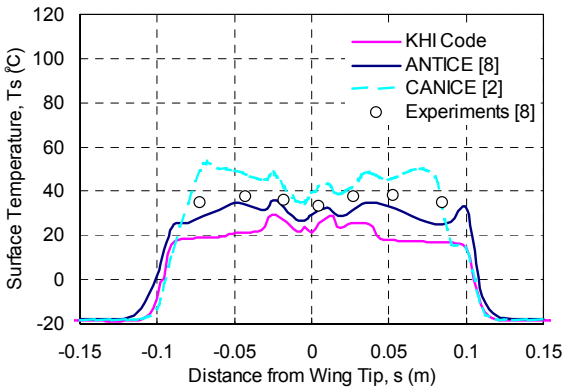

(a) Surface temperature

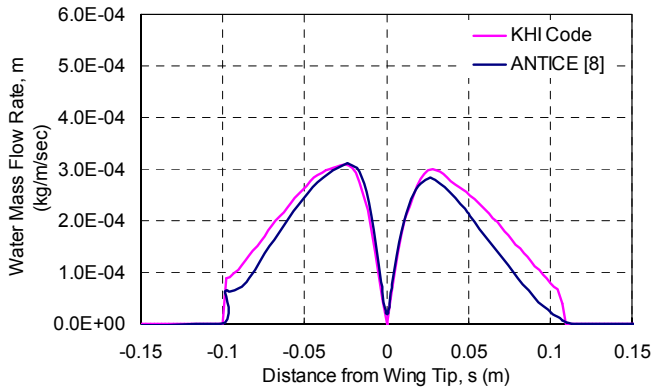

(b) Water mass flow rate

Figure 8 Comparison of experiments and predictions for Case#67A

thickness (0.005 m) were adopted, in the same way as CANICE [2]. In order to neglect the effect of difference of the local collection efficiency calculation, the local collection efficiency calculated by ANTICE, shown in Figure 5, is adopted for the calculation with the KHI code.

The three cases (22A, 35A, and 67A) are evaporative condition that all of the impinging water evaporates in the heating area. The remaining cases (22B and 67B) were running-wet condition that the impinging water runs back behind the heating area. Figures 6-8 show comparison results of the surface temperature and mass flow rate in the evaporative condition. In these cases, the surface temperature around the leading edge calculated by the KHI code comparatively agree with that of the experiments and the ANTICE predictions. The mass flow rates are in excellent agreement with that of the ANTICE predictions. Comparison results in the running-wet condition were shown in Figures 9-10. In these cases, the surface temperature and the mass flow rate distribution with the KHI code agree well with the experiment and ANTICE prediction.

Because of the high water latent heat of evaporation, small difference of the evaporation mass of water affects surface temperature largely. As is seen from the Equation (12), the external heat transfer coefficient affects the water evaporation mass. In the ANTICE calculation, the heat transfer coefficient used the experimental value. KHI code and CANICE used the calculated value of the heat transfer coefficient. The differences of these heat transfer coefficient lead to the differences of the surface temperature.

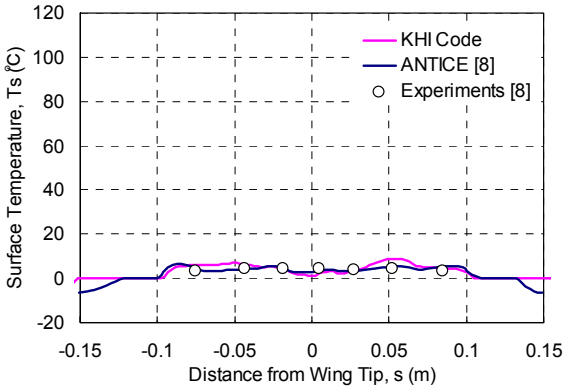

(a) Surface temperature

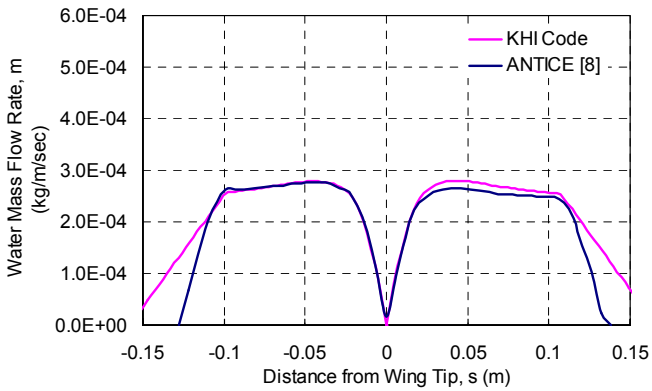

(b) Water mass flow rate

Figure 9 Comparison of experiments and predictions for Case#22B

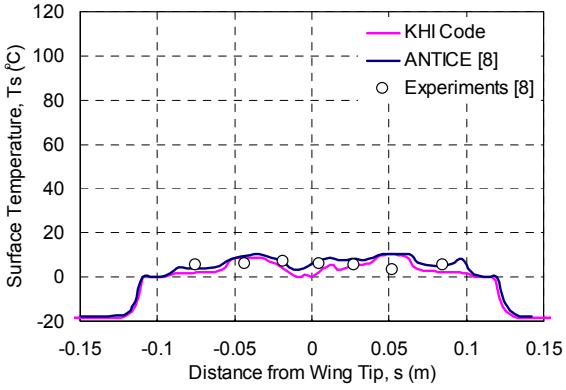

(a) Surface temperature

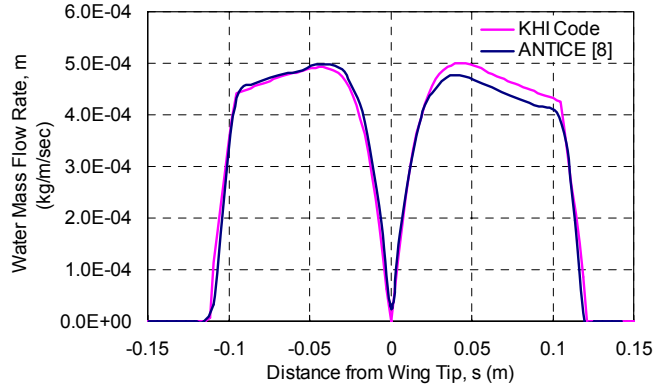

(b) Water mass flow rate

Figure 10 Comparison of experiments and predictions for Case#67B

3.4 Calculation of the Iced Geometry

Figure 11 presents comparisons with the experimental and predicted ice shapes on the NACA0012 airfoil [9]. The experimental data were measured in the NASA Lewis Icing Research Tunnel.

Ice shapes are classified in two categories: rime ice and glaze ice. Rime ice is formed when water droplets freeze on the impact with the aircraft body in the lower temperature condition. Glaze ice is formed by liquid water droplets, which do not freeze immediately on impact. Test conditions for this comparison include rime, mixed, and glaze ice conditions

Multiple time steps were used to predict ice shapes shown in Figure 11. The LEWICE adopted 4 time steps and KHI code did 2 time steps. Ice shapes predicted by the KHI code are similar to experimental ice shapes and ice shapes predicted by the LEWICE, both rime ice and glaze ice. The maximum ice thickness of ice shape with the KHI code are greater than that of experiments and the LEWICE predictions in each condition, because of the conservatism of the KHI code.

4 Conclusions

The KHI code is the two-dimensional ice accretion and anti-icing simulation code. The code consists of four major regions. They are (1) the flow field calculation, (2) the droplet trajectory and impingement calculation, (3) the heat and mass balance calculation, and (4) the ice shape calculation.

Each mathematical model is validated by the experimental data and the numerical results by other simulation codes. These comparisons show that the KHI code can simulate the icing and anti-icing phenomenon as accurately as other simulation codes.

References

[1] Society of Automotive Engineers, "Droplet Impingement and Ice Accretion Computer Codes," *SAE ARP5903*, Oct. 2003.

[2] Morency, F., et al., "Anti-Icing System Simulation Using CANICE," *Journal of Aircraft*, Vol. 36, No. 6, pp 999-1006, 1999.

[3] Ruff, G.A. and Berkowiz B.M., "Users Manual for the NASA Lewis Ice Accretion Prediction code (LEWICE)," *NASA CR 185129*, May 1990.

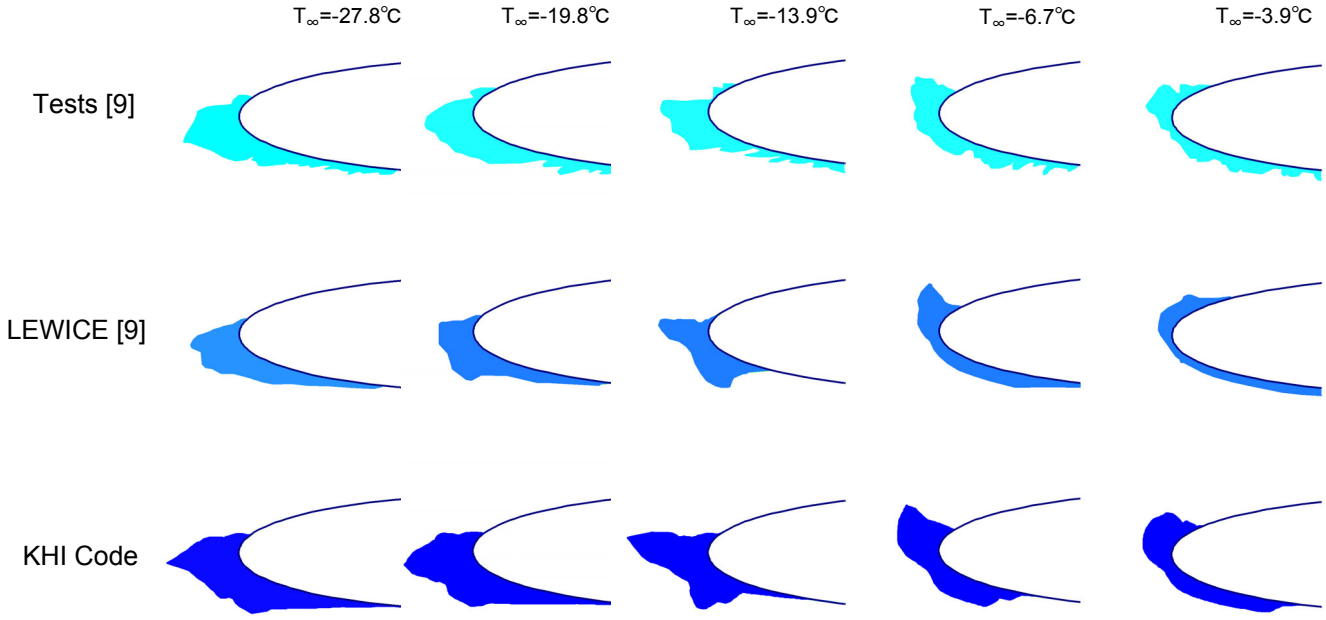

Figure 11 Comparison of ice shape predictions and experiments

[4] *JSME Data Book*: Heat Transfer 4th Edition, 1986. (in Japanese)

[5] Harris C. D., "Two-Dimensional Aerodynamic Characteristics of the NACA0012 Airfoil in the Langley 8-foot Transonic Pressure Tunnel," *NASA TM-81927*, April 1981.

[6] Paradakis M., et al., "Methods for Obtaining and Reducing Experimental Droplet Impingement Data on Arbitrary Bodies," *Journal of Aircraft*, Vol. 28, No. 5, pp328-336, May 1991.

[7] Miller D., et al., "Validation of NASA Thermal Ice Protection Computer Codes Part 1 – Program Overview," *AIAA97-0049*, Jan. 1997.

[8] Al-Khalil, K., et al., "Validation of Thermal Ice Protection Computer Codes: Part 3 – The Validation of ANTICE," *AIAA 97-0051*, Jan. 1997.

[9] Wright W. B., et al., "DRA/NASA/ONERA Collaboration on Icing Research, Part II – Prediction of Airfoil Ice Accretion," *NACA CR-202349*, 1997.

[10] Morency, F., et al., "Heat and Mass Transfer in the Case of Anti-Icing System Simulation," *Journal of Aircraft*, Vol. 37, No.2, pp.245-252, 2000.